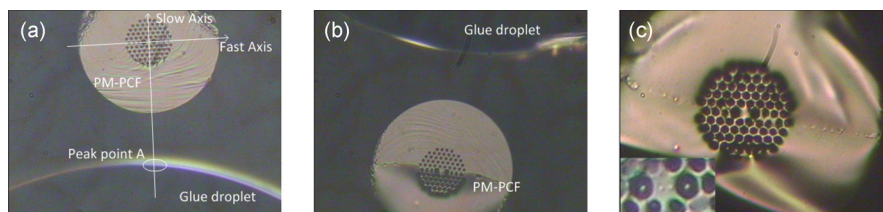


Temperature Sensor by Using Selectively Filled Photonic Crystal Fiber Sagnac Interferometer

Volume 4, Number 5, October 2012

Ying Cui
Perry Ping Shum
Dora Juan Juan Hu
Guanghui Wang
Georges Humbert
Xuan-Quyen Dinh



DOI: 10.1109/JPHOT.2012.2217945
1943-0655/\$31.00 ©2012 IEEE

Temperature Sensor by Using Selectively Filled Photonic Crystal Fiber Sagnac Interferometer

Ying Cui,^{1,2} Perry Ping Shum,^{1,2} Dora Juan Juan Hu,³ Guanghui Wang,⁴
Georges Humbert,⁵ and Xuan-Quyên Dinh^{1,6}

¹CINTRA CNRS/NTU/THALES, UMI 3288, Singapore 637553

²School of Electrical and Electronic Engineering, Nanyang Technological University, Singapore 639798

³Institute for Infocomm Research, Agency for Science, Technology, and Research, Singapore 138632

⁴Department of Electronic Engineering, The Chinese University of Hong Kong, Shatin, Hong Kong

⁵Xlim-UMR 6172, University of Limoges/CNRS, 87060 Limoges Cedex, France

⁶Thales Solutions Asia Pte Ltd., Singapore 498788

DOI: 10.1109/JPHOT.2012.2217945
1943-0655/\$31.00 ©2012 IEEE

Manuscript received July 14, 2012; revised September 1, 2012; accepted September 4, 2012. Date of publication September 10, 2012; date of current version September 20, 2012. Corresponding author: P. P. Shum (e-mail: shum@ieee.org).

Abstract: In this paper, we report an optical fiber Sagnac interferometer (OFSI)-based temperature sensor constructed by a selectively filled polarization-maintaining photonic crystal fiber (PM-PCF). The transmission spectrum of the OFSI is in sinusoidal form and is sensitive to temperature. Simulation results predicted a higher sensitivity by selective filling than nonselective filling. In experiments, we used an extremely low-cost process to realize the selective filling. A sensitivity of 2.58 nm/°C was achieved with an 11.7-cm-long PM-PCF. The sensitivity dependence on the infiltration length ratio was also investigated.

Index Terms: Sagnac interferometer, temperature sensor, photonic crystal fiber, selective filling.

1. Introduction

In the recent decades, great attention has been paid to a new category of optical fibers, photonic crystal fibers (PCFs), the cladding of which contains a periodic structure of air holes running along the whole length of the fibers, forming 2-D photonic crystals. The existence of these air holes provides various engineering potentials of the fibers and enables special properties, such as high birefringence, endlessly single mode, large mode area, large dispersion, and special temperature responses [1].

The polarization-maintaining photonic crystal fiber (PM-PCF) is a kind of PCF with higher birefringence than traditional polarization-maintaining fibers, allowing a shorter length in practical use [2]. Optical fiber Sagnac interferometers (OFSIs) [3] constructed by the PM-PCF have been developed into various optical sensors with merits of compact configuration, high performance, and ease of fabrication [4]. However, most of these sensors are almost temperature insensitive since the PM-PCF is composed of a single material and has a weak temperature response [3], [5]–[7].

Besides the design of air hole arrays, there is a trend to tailor the PCF properties by postprocessing of infiltration. A variety of liquids, such as aqueous solutions, index oils [8], [9], polymers [10], liquid crystals [11]–[13], and even metals [14], have been employed to fulfill applications of optical sensing, switching, or communications. A high-sensitivity temperature sensor was reported using nonselective infiltration of alcohol in PCF. A recent work [8] has reported the infiltration of high-index

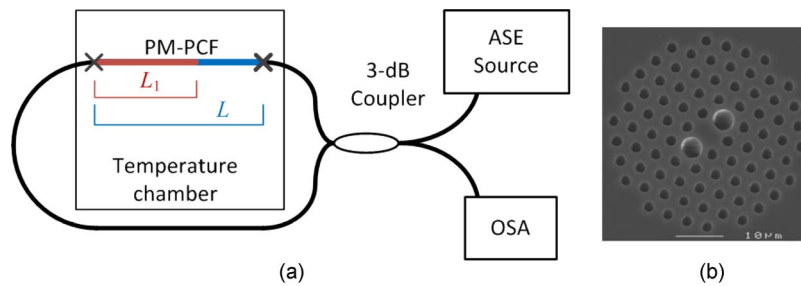


Fig. 1. (a) Schematic diagram of the OFSI-based temperature sensor. L_1 is the infiltration length, and L is the total length of PM-PCF inside the fiber loop. (b) SEM image of the cross section of the PM-PCF used.

liquid in PM-PCF converting it into a band-gap fiber. A temperature sensitivity of $0.4 \text{ nm}/^\circ\text{C}$ was achieved. In recent years, there have been some temperature sensors based on modal coupling. For example, in [15], a dual-core fiber was filled with high-index liquid, and a sensitivity of $1.9 \text{ nm}/^\circ\text{C}$ was achieved; In [9], one of the cladding holes is filled with 1.46 index liquid, and the core mode is coupled to the liquid mode. An ultrahigh sensitivity was achieved. However, both sensors suffer from narrow dynamic ranges, which are limited to only a few degrees.

The nonselective filling of most liquids can be done by simply immersing the PCF tip in the liquid. However, the selective filling, which can give better performance or more interesting phenomena, normally requires a complex process like several times of injection–cure–cleave step using UV curable polymer [10], deposition and drilling using femtosecond laser [16], or attachment of adhesive on specific voids using an ultrasmall optical fiber tip [14].

In this paper, we used a simplified process, which is extremely low cost and easy to operate, to realize the selective filling. Water was infiltrated into only the two big holes of the PM-PCF, the pattern predicted by simulation analysis giving the most improvement in sensitivity than nonselective filling. Since the index of water is lower than the fiber material silica, index guiding of light is maintained. With the presence of water, the OFSI showed a high temperature sensitivity based on the thermal-induced birefringence change as well as a wide dynamic range and flexibility. The experiment results of an 11.7-cm-long PM-PCF realized a sensitivity of $2.58 \text{ nm}/^\circ\text{C}$. The influence of infiltration length on the OFSI sensitivity was also experimentally demonstrated for the first time.

2. Working Principle

The fundamental working principle of the proposed temperature sensor is based on the birefringence dependence of the selectively filled PM-PCF on temperature. Since liquids, such as water or ethanol, have much higher thermal expansion coefficients than solid silica, the fiber material, the effective refractive indices for slow and fast axes of the selectively filled PM-PCF change significantly with temperature, therefore leading to a birefringence change of the selectively filled PM-PCF. This temperature-induced birefringence change is detected by the OFSI and present in the form of a spectrum shift.

2.1. Mechanism of OFSI

The schematic illustration of the OFSI-based temperature sensor is shown in Fig. 1(a). Fig. 1(b) shows the cross section of the PM-PCF used. There are two big air holes along one axis of the cross section and a number of small holes in other parts of the cladding. The noncentrosymmetric arrangement of air holes leads to the birefringence of the PM-PCF. The OFSI is an optical fiber loop composed of a piece of selectively filled PM-PCF with both ends connected to a 3-dB coupler. The input of the OFSI is connected to a light source, and the output is connected to an optical spectrum analyzer (OSA). The PM-PCF is placed in a temperature chamber to experience the temperature change. Suppose the total PM-PCF length inside the fiber loop is L , the selectively filled length is L_1 , and the whole length of PM-PCF is inside the temperature chamber.

The sensing mechanism of the OFSI is given as follows: First, light is launched from the light source into the optical fiber loop. Then, the light is split into two waves when passing through the 3-dB coupler. One sub-beam propagates clockwise in the fiber loop, while the other sub-beam propagates counterclockwise. The two sub-beams experience different optical path lengths because of the birefringence of the selectively filled PM-PCF, however, carrying on the same original frequency. Sharing a phase difference, the two sub-beams interfere with each other when they recombine at the coupler. The phase difference is given by

$$\psi = 2\pi BL/\lambda \quad (1)$$

where B is the birefringence of the selectively filled PM-PCF, L is the total length of the PM-PCF, and λ is the wavelength of light. The transmission spectrum of the fiber loop is therefore approximately a sinusoidal function of wavelength, which can be described by the following equation [2]:

$$T = (1 - \cos\psi)/2. \quad (2)$$

If the condition $\psi = 2\pi m$ is fulfilled, the transmission spectrum will reach its maxima. m is an integer and represents the fringe order. Therefore, the dip wavelength of the m th order is given by

$$\lambda_m = BL/m. \quad (3)$$

We can derive the free spectral range, i.e., the wavelength spacing S between the two adjacent dips as

$$S = \frac{\lambda^2}{BL}. \quad (4)$$

When the temperature changes, the thermal effect of the unfilled part of the PM-PCF can be neglected due to the extremely small temperature response [5]. The birefringence change ΔB at the infiltrated part of the PM-PCF with length L_1 contributes to the phase shift of the OFSI the most, which can be expressed as follows:

$$\Delta\psi = 2\pi\Delta BL_1/\lambda. \quad (5)$$

Therefore, the wavelength shift caused by temperature change for a certain wavelength is given by

$$\Delta\lambda = \lambda \frac{\Delta B L_1}{B L}. \quad (6)$$

Regarding simulation exploration of the selective filling pattern, the one giving a larger relative birefringence change $\Delta B/B$ under the same liquid index change will provide a larger wavelength shift, thus a higher sensitivity. For experiment investigation on how the PM-PCF length influences the sensitivity, the equation shows that the sensitivity is proportional to the infiltration length ratio over the total PM-PCF length L_1/L .

2.2. Mechanism for Infiltration

The infiltration of liquid into voids of the PM-PCF is realized by capillary action. The capillary force for a certain air hole is given by [14]

$$F_c = 2\pi a\sigma \cos\theta \quad (7)$$

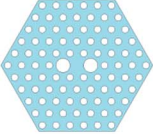
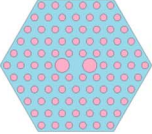
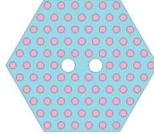
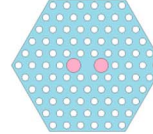
where a is the radius of the air hole, σ is the liquid–air surface tension, and θ is the contact angle between the liquid and the silica wall. Considering gravity, the achievable height of the liquid column supported by the capillary action is

$$h = \frac{2\sigma \cos\theta}{\rho g a} \quad (8)$$

where ρ is the density of liquid, and g is the local gravitational field strength.

TABLE 1

Birefringence and relative birefringence change of different infiltration patterns

	<i>No infiltration</i>	<i>All holes liquid</i>	<i>Small holes liquid</i>	<i>Big holes liquid</i>
Infiltration Pattern				
$B_{1.33}(10^{-4})$	5.436	2.111	4.825	1.999
$B_{1.36}(10^{-4})$	5.436	1.610	3.944	1.455
$\Delta B/B$	0	23.7%	18.3%	27.2%

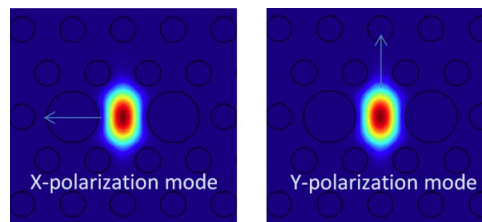


Fig. 2. Mode fields of two orthogonal fundamental modes supported by the waveguide.

In the case of water-filled PM-PCF holes, radius a is $2.25 \mu\text{m}$, σ is around 72 mN/m at a room temperature of 25°C , θ is around 30° , ρ is 1000 kg/m^3 , and g is 9.81 m/s^2 . The corresponding height of the water column is 5.6 m , which is much longer than the PM-PCF length used in the experiments. Therefore, we do not need to apply pressure to push water into the PM-PCF. By blocking all other air holes and positioning the fiber tip in water, water will be drawn into the opened voids of the PM-PCF by capillary force.

3. Simulation Results

In order to find an optimized pattern of infiltration, the birefringence of the PM-PCF with different infiltration patterns was investigated using a finite-element method. The geometry of the simulation model is shown in the pictures of Table 1. The diameters of the big and small holes are $4.5 \mu\text{m}$ and $2.2 \mu\text{m}$, respectively, and the pitch is $4.4 \mu\text{m}$ based on the parameters of the PM-PCF used in the experiments. The refractive indices of silica and air are set to be 1.45 and 1. Since the refractive index of liquid varies with temperature, it is set to be 1.33 and 1.36 separately in different simulations to investigate the corresponding birefringence change.

These pictures in Table 1 also show different infiltration patterns, including all holes infiltrated, only the small holes infiltrated and only the big holes infiltrated. The blue hexagon represents silica, the white circles represent air holes, and the pink circles represent liquid-filled holes. For each pattern, there are two orthogonal fundamental modes supported by the waveguide structure, as shown in Fig. 2. By comparing the effective refractive indices of the two modes, the birefringence of the waveguide can be found.

According to (6), the sensitivity of the proposed sensor is proportional to the relative birefringence change $\Delta B/B$; therefore, the values of $\Delta B/B$ were investigated for different infiltration patterns, where ΔB is the birefringence change under a liquid index change from 1.33 to 1.36, and B is the birefringence under the liquid index of 1.33.

The achieved birefringence and relative birefringence change values are shown in Table 1, from which we can tell that the presence of liquid significantly decreases the birefringence of the PM-PCF.

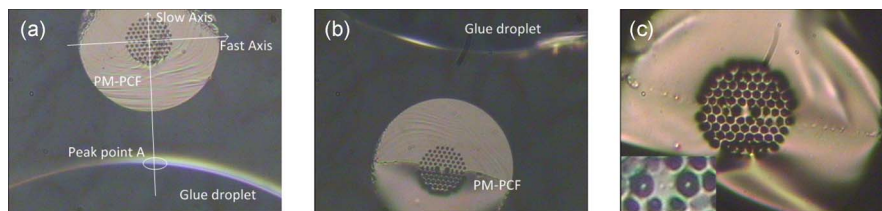


Fig. 3. Microscopic images of (a) clean PM-PCF and the glue droplet, (b) half-covered PM-PCF and the glue droplet, and (c) PM-PCF with all small holes covered; inset: the cross section after liquid infiltration.

Especially when the big holes are infiltrated, the birefringence value decreases by more than half. With the change of the liquid index, the pattern of only the big holes infiltrated provides the largest relative birefringence change of 27.2%, thus giving the best sensitivity. Therefore, in the experiments, we infiltrated only the big holes of the PM-PCF to achieve a better sensitivity.

4. Fabrication

The proposed temperature sensor is fabricated by first blocking the small holes; then immersing the PM-PCF tip in water; and after a while, splicing it with the 3-dB coupler.

The PM-PCF used is a commercial product from Blaze Photonics. In the process of blocking, we use the common glue that we can find in the stationery store and an ordinary single-mode fiber, which does not need to be tapered as required by other methods [14]. The process is stated as follows.

A piece of well-cleaved PM-PCF is vertically fixed under a microscope. Another single-mode fiber is horizontally fixed on a multidimensional translation stage with a drop of liquid glue attached on its tip. We tune the stage slowly to make the glue droplet approach the end face of the PM-PCF. Once the glue droplet comes into view of the microscope, it is crucial to make sure that the slow axis of the PM-PCF goes through the peak point of the droplet hemisphere (point A indicated in the figure), as shown in Fig. 3(a), before further moving forward the droplet to touch the PM-PCF end face. This way, the glue can spread on the end face in an axisymmetric manner.

The motion of the glue is monitored under the microscope. The objective lens we used is 20 \times in order to be able to observe the PM-PCF and the glue droplet in the same screen. Once the glue has covered the half number of the small holes, we remove the single-mode fiber promptly. The glue then stops flowing and stays at the PM-PCF end face, as shown in the bottom part in Fig. 3(b). Repeat the process to get the other half number of the small holes covered by the glue. With the existence of glue on top, the small holes look magnified in the microscopic image shown in Fig. 3(c), and the big holes keep the original size since they are left open.

We wait for a short while for the glue to dry up. Then, the treated fiber tip is immersed in DI water, and the infiltration is automatically done by capillary action. We use water as the infiltration liquid because it is the most commonly available liquid with a high thermal expansion coefficient and not as easy to evaporate as ethanol. The inset in Fig. 3(c) shows the same PM-PCF end face after infiltration. The glue is still present since the small holes still look magnified. Water is filled inside the big holes as indicated by the bright dots in the big holes. A PM-PCF sample with only the big holes infiltrated with water is therefore ready for measurement. This process is extremely low cost since it does not involve a special material or component. It can be done within one minute after only a few times practice.

Finally, the proposed sensor is built by cleaving both ends of the PM-PCF and connecting it with two ports of a 3-dB coupler by fusion arc splicing.

5. Experiment Results and Discussion

Experiments were carried out to investigate the performance of the proposed sensor. The experiment setup is shown in Fig. 1. We use an amplified spontaneous emission (ASE) source with a

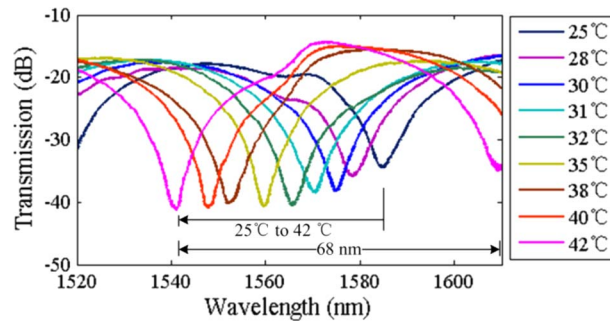


Fig. 4. Transmission spectra of the OFSI under different temperatures.

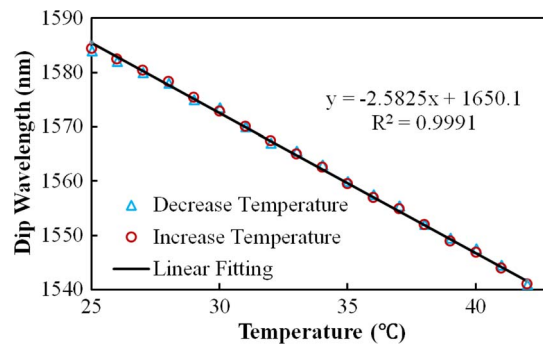


Fig. 5. Dip wavelengths of the spectrum under different temperatures.

wavelength range of 1520–1610 nm to launch light into the OFSI and an OSA with a resolution of 0.02 nm to monitor the transmission spectra.

5.1. Performance of the Temperature Sensor

An OFSI with a piece of selectively filled PM-PCF of 11.7 cm with the whole length infiltrated is examined. The PM-PCF was placed in a temperature chamber to experience different temperatures. The transmission spectra under different temperatures are shown in Fig. 4. The total insertion loss of the OFSI is around 15 dB, which is mainly due to the mode field mismatch between single-mode fibers and the PM-PCF. Since only the two big holes were filled with liquid, the insertion loss is much lower than that in [8]. The transmission spectrum at a certain temperature is a periodic function of wavelength, but only one dip appears in the light source range. From the spectrum of 42 °C, we can approximate that the spacing between transmission dips is around 68 nm. The large spacing is due to, first, a relatively short PM-PCF length and, second, a reduction of birefringence caused by the infiltration as predicted by simulation analysis. The extinction ratio is around 25 dB.

With the increase in the temperature from 25 °C to 42 °C, the transmission dip shifts to a shorter wavelength from 1584 nm to 1541 nm. With the cooling down of the temperature chamber, the spectral dip shifts back to the longer wavelength. The dip wavelength as a function of temperature is shown in Fig. 5. The dip wavelengths of increasing and decreasing temperatures almost overlap with each other, indicating high stability and repeatability of the proposed sensor. Linear curve fitting of the experiment data gives a sensitivity of 2.58 nm/°C with a good linearity. The sensitivity is much higher than traditional polarization-maintaining-fiber-based sensors (~ 0.94 nm/°C) and fiber-Bragg-grating-based temperature sensors (~ 0.01 nm/°C) [2]. The resolution of the proposed sensor is mainly restricted by the resolution of the OSA. Nowadays, one can easily find an OSA with a resolution of 10 pm. The corresponding resolution of the proposed sensor is therefore

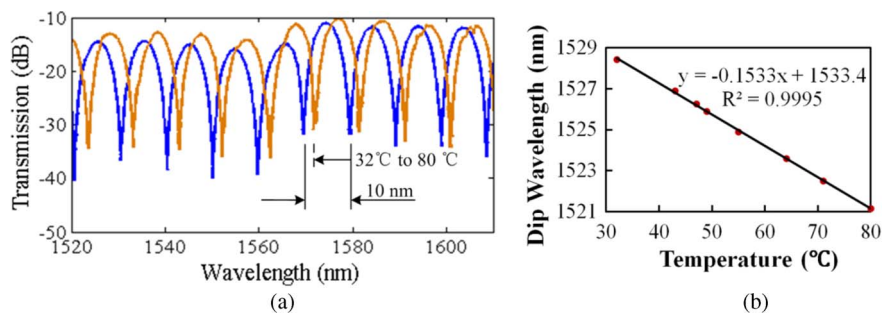


Fig. 6. (a) Transmission spectra of the OFSI with 44-cm PM-PCF under different temperatures. (b) Dip wavelength against temperature curve giving the sensitivity.

around $0.004\text{ }^{\circ}\text{C}$, which is sufficiently small compared with commercialized thermometers. The operational range of the proposed sensor is limited by the wavelength spacing S between the adjacent transmission dips on the transmission spectrum, which is about 68 nm , as shown in Fig. 4. As predicted by (4), this operational range of the proposed sensor can be further improved by using a shorter length of PMF-PCF to increase the wavelength spacing S . Meanwhile, the spectral range of the light source used in the experiment is less than 100 nm (ASE source, $1520\text{--}1620\text{ nm}$). In order to achieve a broader spectral range for the sensor, a supercontinuum source ($600\text{--}1700\text{ nm}$) can be used accordingly. The bandwidth of the 3-dB coupler is another potential limitation for the operational range of the sensor, which is typically about 30 nm for a common fiber coupler and 80 nm for a broadband fiber coupler. This restriction can be eliminated by using the setup based on the polarization interferometer, which can avoid using the coupler [17].

5.2. Effect of Infiltration Length Ratio

The temperature response of another sample with shorter infiltration length and longer total length was examined using the same configuration. Only a short part of the total length of 44 cm was infiltrated with water. Fig. 6(a) shows the transmission spectra of the OFSI at $32\text{ }^{\circ}\text{C}$ (blue curve) and $80\text{ }^{\circ}\text{C}$ (yellow curve). The insertion loss is around 10 dB , and the extinction ratio is around 25 dB . It shows clearly that the transmission is a periodic function of wavelength with many transmission dips. The spacing is 10 nm , which is much smaller than that of the previous sample because the PM-PCF length is much longer.

With the increase in temperature from $32\text{ }^{\circ}\text{C}$ to $80\text{ }^{\circ}\text{C}$, the transmission dips shifted to shorter wavelengths for about 7 nm . We use the dip around 1530 nm as an example to explore the sensitivity of this sample. Linear curve fitting of the experiment data of the dip wavelength against temperature is shown in Fig. 6(b). The achieved sensitivity is about $0.15\text{ nm}/^{\circ}\text{C}$. On the one hand, this value is much larger than the temperature sensitivity of the PM-PCF without any infiltration ($0.29\text{ pm}/^{\circ}\text{C}$) [5], which confirms that there is water inside the fiber; on the other hand, the value is one order of magnitude smaller than that of the previous sample, i.e., the PM-PCF with the whole length infiltrated, which agrees with the theoretical analysis that a higher infiltration length ratio provides a higher sensitivity.

Calibration is suggested before using the proposed sensor. The variations of PM-PCF length and infiltration length ratio from sensor to sensor in real experiments lead to different dip wavelengths in transmission spectra. The sensitivity is also dependent on the dip wavelength indicated by (6). Therefore, the performance of each sensor can be slightly different from other sensors with similar parameters. After calibration, the behavior of the proposed sensor is much more predictable by the calibration curve.

6. Conclusion

In conclusion, we proposed a high-sensitivity temperature sensor by using selectively filled PM-PCFs. From simulation analysis, an optimized infiltration pattern giving the most improvement in

sensitivity was found. The infiltration pattern was realized by a simplified process in experiment. Experiment investigations showed a sensitivity of $2.58 \text{ nm}/^\circ\text{C}$ of the proposed sensor. By comparison of sensitivities of samples with different infiltration length ratios, we found that the sensitivity of the proposed sensor was proportional to the PM-PCF infiltration length ratio, which agrees with the theoretical analysis.

References

- [1] W. W. Qian, C. L. Zhao, S. L. He, X. Y. Dong, S. Q. Zhang, Z. X. Zhang, S. Z. Jin, J. T. Guo, and H. F. Wei, "High-sensitivity temperature sensor based on an alcohol-filled photonic crystal fiber loop mirror," *Opt. Lett.*, vol. 36, no. 9, pp. 1548–1550, May 2011.
- [2] Y. Liu, B. Liu, X. H. Feng, W. G. Zhang, G. Zhou, S. Z. Yuan, G. Y. Kai, and X. Y. Dong, "High-birefringence fiber loop mirrors and their applications as sensors," *Appl. Opt.*, vol. 44, no. 12, pp. 2382–2390, Apr. 2005.
- [3] C. L. Zhao, X. F. Yang, C. Lu, W. Jin, and M. S. Demokan, "Temperature-insensitive interferometer using a highly birefringent photonic crystal fiber loop mirror," *IEEE Photon. Technol. Lett.*, vol. 16, no. 11, pp. 2535–2537, Nov. 2004.
- [4] P. Zu, C. C. Chan, L. W. Siang, Y. X. Jin, Y. F. Zhang, L. H. Fen, L. H. Chen, and X. Y. Dong, "Magneto-optic fiber Sagnac modulator based on magnetic fluids," *Opt. Lett.*, vol. 36, no. 8, pp. 1425–1427, Apr. 2011.
- [5] X. Y. Dong, H. Y. Tam, and P. Shum, "Temperature-insensitive strain sensor with polarization-maintaining photonic crystal fiber based Sagnac interferometer," *Appl. Phys. Lett.*, vol. 90, no. 15, pp. 151113-1–151113-3, Apr. 2007.
- [6] R. M. Silva, M. S. Ferreira, and O. Frazao, "Temperature independent torsion sensor using a high-birefringent Sagnac loop interferometer," *Opt. Commun.*, vol. 285, no. 6, pp. 1167–1170, Mar. 2012.
- [7] P. Zu, C. C. Chan, Y. X. Jin, Y. F. Zhang, and X. Y. Dong, "Fabrication of a temperature-insensitive transverse mechanical load sensor by using a photonic crystal fiber-based Sagnac loop," *Meas. Sci. Technol.*, vol. 22, no. 2, pp. 025204-1–025204-4, Feb. 2011.
- [8] X. B. Zheng, Y. G. Liu, Z. Wang, T. T. Han, C. L. Wei, and J. J. Chen, "Transmission and temperature sensing characteristics of a selectively liquid-filled photonic-bandgap-fiber-based Sagnac interferometer," *Appl. Phys. Lett.*, vol. 100, no. 14, pp. 141104-1–141104-4, Apr. 2012.
- [9] Y. Wang, M. W. Yang, D. N. Wang, and C. R. Liao, "Selectively infiltrated photonic crystal fiber with ultrahigh temperature sensitivity," *IEEE Photon. Technol. Lett.*, vol. 23, no. 20, pp. 1520–1522, Oct. 2011.
- [10] Y. Y. Huang, Y. Xu, and A. Yariv, "Fabrication of functional microstructured optical fibers through a selective-filling technique," *Appl. Phys. Lett.*, vol. 85, no. 22, pp. 5182–5184, Nov. 2004.
- [11] J. J. Hu, P. Shum, G. B. Ren, X. Yu, G. H. Wang, C. Lu, S. Ertman, and T. R. Wolinski, "Investigation of thermal influence on the bandgap properties of liquid-crystal photonic crystal fibers," *Opt. Commun.*, vol. 281, no. 17, pp. 4339–4342, Sep. 2008.
- [12] J. J. Hu, G. B. Ren, P. Shum, X. Yu, G. H. Wang, and C. Lu, "Analytical method for band structure calculation of photonic crystal fibers filled with liquid crystal," *Opt. Exp.*, vol. 16, no. 9, pp. 6668–6674, Apr. 2008.
- [13] D. Hu, J. Lim, Y. Cui, K. Milenko, Y. Wang, P. Shum, and T. Wolinski, "Fabrication and characterization of a highly temperature sensitive device based on nematic liquid crystal filled photonic crystal fiber," *IEEE Photon. J.*, vol. 4, no. 5, pp. 1248–1255, Oct. 2012.
- [14] R. Spittel, D. Hoh, S. Bruckner, A. Schwuchow, K. Schuster, J. Kobelke, and H. Bartelt, "Selective filling of metals into photonic crystal fibers," in *Proc. Photon. Phononic Properties Eng. Nanostruct.*, vol. 7946, A. Adibi, S. Y. Lin, and A. Scherer, Eds., 2011, vol. 7946, pp. 79460Z-1–79460Z-8.
- [15] J. B. Du, Y. G. Liu, Z. Wang, Z. Y. Liu, B. Zou, L. Jin, B. Liu, G. Y. Kai, and X. Y. Dong, "Thermally tunable dual-core photonic bandgap fiber based on the infusion of a temperature-responsive liquid," *Opt. Exp.*, vol. 16, no. 6, pp. 4263–4269, Mar. 2008.
- [16] J. A. Ju, H. F. Xuan, W. Jin, S. J. Liu, and H. L. Ho, "Selective opening of airholes in photonic crystal fiber," *Opt. Lett.*, vol. 35, no. 23, pp. 3886–3888, Dec. 2010.
- [17] P. Zu, C. C. Chan, W. S. Lew, Y. X. Jin, H. F. Liew, L. H. Chen, W. C. Wong, and X. Y. Dong, "High extinction ratio magneto-optical fiber modulator based on nanoparticle magnetic fluids," *IEEE Photon. J.*, vol. 4, no. 4, pp. 1140–1146, Aug. 2012.